Organic Electronics 15 (2014) 517–523

Contents lists available at ScienceDirect

Organic Electronics

journal homepage: www.elsevier.com/locate/orgel

Single-emission-layer white organic light-emitting devices: Chromaticity and colour-rendering consideration

Chia-Chan Fan [a], Ming-Hong Huang [a], Wei-Chieh Lin [a], Hao-Wu Lin [a,*], Yun Chi [b], Hsin-Fei Meng [c], Teng-Chih Chao [d], Mei-Rurng Tseng [d]

[a] Department of Materials Science and Engineering, National Tsing Hua University, Hsin Chu, Taiwan
[b] Department of Chemistry, National Tsing Hua University, Hsin Chu, Taiwan
[c] Institute of Physics, National Chiao Tung University, Hsin Chu, Taiwan
[d] Material and Chemical Research Laboratories, Industrial Technology Research Institute (ITRI), Hsin Chu, Taiwan

ARTICLE INFO

Article history:
Received 6 October 2013
Received in revised form 13 November 2013
Accepted 30 November 2013
Available online 12 December 2013

Keywords:
Solution-processed
Organic light-emitting diodes
Colour-rendering index
Daylight locus

ABSTRACT

The chromaticity and colour-rendering capability of solution-processed single emission layer (EML) white organic light-emitting diodes (W-OLEDs) can be precisely tuned by manipulating the dopant compositions in the EMLs. In this work, we numerically modelled binary, ternary, and quaternary doping single EML W-OLEDs. The correlated colour temperature (CCT), colour-rendering index (CRI), and spectral designs were correlated. The simulation predicted that the quaternary doping system possesses the best chromaticity performance. The corresponding binary, ternary and quaternary doping single EML W-OLEDs were fabricated and characterised to verify the calculation. The solution-processed quaternary doping W-OLEDs were designed with CRI values up to 85, deviations from the Planckian locus ($D_{u'v'}$) as low as +0.0009, an EQE of 13.7%, a power efficacy of 14.7 lm/W and current efficiency of up to 24.9 cd/A at 1000 cd/m^2.

1. Introduction

White organic light-emitting devices (W-OLEDs) based on solution processes exhibit both high reproducibility and material utilisation, which make them promising candidates for large-area, low-cost solid-state lighting [1–8]. To prevent interfacial mixing, the single emission layer (EML) that consists of a host and multi-colour dopants is usually adopted in solution processed W-OLEDs [1–3]. Due to this unique characteristic, solution-processed W-OLEDs constitute a high-quality lighting source (*e.g.*, high colour rendering index (CRI), target correlated colour temperature (CCT) and small deviation ($D_{u'v'}$) from Planckian locus in CIE 1976 coordinates) with different approaches than their thermal-evaporation counterparts. In thermal-evaporation W-OLEDs, the stacking of multi-EMLs in which a single EML consists of one host and one emissive dopant is commonly utilised to achieve the required illumination quality [9–17]. This approach is adopted because controlling the ratio of compositions (1 host and $\geqslant$2 dopants) for multiple sources of co-deposition is difficult. Conversely, the ratios of various components can be precisely controlled in solution processes by varying the weight percentage of dissolved materials [18–20]. Furthermore, the colour-shift under different operational current densities can be prohibited in solution processed single EML W-OLEDs because of their spatial homogeneity in the emission zone [21,22]. However, the mechanism by which the manipulation of the EML of solution processed W-OLEDs increases the illumination quality has not been revealed. In this study, we investigated the chromaticity and the colour-rendering performance of single EML solution-processed W-OLEDs based on commercial available emission dopants (*e.g.*, red emitter Osmium(II)bis(5-(benzothiazol-2-yl)-3-trifluoromethylpyrazole)1,2-bis(phospholano)benzene (Os(btfp)$_2$(pp2b),

* Corresponding author. Tel.: +886 3 5715131x33879.
E-mail address: hwlin@mx.nthu.edu.tw (H.-W. Lin).

1566-1199/$ - see front matter © 2013 Elsevier B.V. All rights reserved.
http://dx.doi.org/10.1016/j.orgel.2013.11.040

yellow emitter Iridium(III)bis(4-phenylthieno [3,2-c]pyridinato-N,C^2) (PO-01-TB), green emitter iridium(III)tris (2-(4-tolyl)phenylpyridine) ($Ir(mppy)_3$), and blue emitter Bis[2-(4,6-difluorophenyl)pyridinato-C^2,N](picolinato)iridium(III) (FIrpic)) [23–26]. The illumination characteristics were first simulated by superimposing the electroluminescence (EL) spectra of individual monochromatic devices. For binary-emissive dopant (red R and blue B) devices, only one R:B combination can fall on the Planckian locus. Both the simulation and experimental results indicate that this type of device shows a high CCT value but a poor colour-rendering capability. To increase the CRI, green (G) or yellow (Y) emissive-dopants must be introduced inside the EMLs. Multiple possibilities of R:G:B, R:Y:B or R:G:Y:B combinations fit well with the requirement of a small $D_{u'v'}$ value [27,28]. However, these combinations show various CCT and CRI characteristics. A correlation between the initial R:B ratio (before adding G or Y parts), the CRI and CCT was determined. R:B, R:G:B, R:Y:B and R:G:Y:B devices whose emission spectra approach the numerical design were fabricated. The experimental results closely approximate the simulation values. The R:B devices produced white emission with a Commission internationale de l'éclairage (CIE) 1931 coordinates of (0.33, 0.34), external quantum efficiency (EQE) of 13.2%, current efficiency of 22.6 cd/A, power efficacy of 13.1 lm/W, and CRI of 59 at 1000 cd/m^2. The R:G:B and R:Y:B W-OLEDs (CCT ~ 3000 K) exhibited an improved CRI of 79. Finally, the R:G:Y:B devices exhibited an excellent CRI value up to 85 and very low $D_{u'v'}$ values as low as + 0.0009 and a CCT = 2699 K, accompanied with an acceptable EQE of 13.7%, current efficiency of 24.9 cd/A and power efficacy of 14.7 lm/W at 1000 cd/m^2.

2. Results and discussion

2.1. Photophysical properties

The molecular structures of the host and emissive dopants used in the EMLs are shown in Fig. 1. The monochromatic OLEDs were fabricated first. The device structure was optimised as follows (optimisation procedures see Supporting Information S1): indium tin oxide (ITO)/Poly(3,4-ethylenedioxythiophene:poly(styrenesulfonate) (PEDOT:PSS) (40 nm)/ 4,4′,4″-tris(N-carbazolyl)-triphenylamine (TCTA) (40 nm)/ 2,6-bis[(3-carbazol-9-yl)phenyl)]pyridine (26DCzPPy): dopants (30 nm)/1,3,5-tri(m-pyrid-3-yl-phenyl)-benzene (TmPyPB) (50 nm)/CsF (1 nm)/Al (140 nm). The EL spectra and the corresponding CIE 1931 coordinates of red, yellow, green and blue devices are shown in Fig. 2a. The EL spectra

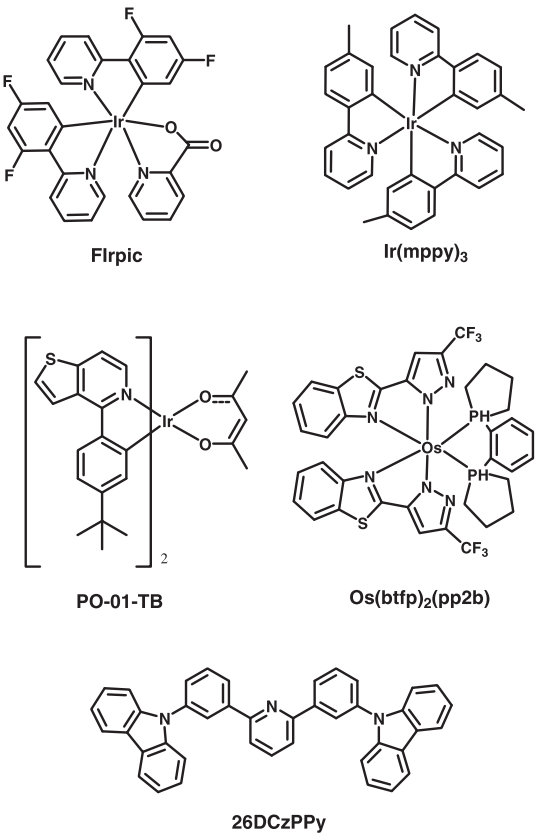

Fig. 1. The molecular structures of dopants (Firpic, $Ir(mppy)_3$, PO-01-TB, and $Os(btfp)_2(pp2b)$) and host (26DCzPPy) used in the EMLs.

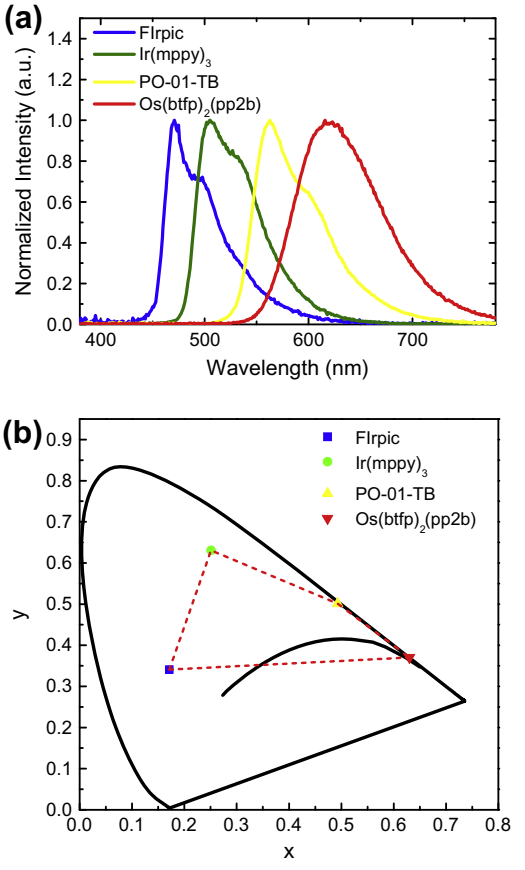

Fig. 2. (a) The electroluminescence spectra and (b) their corresponding chromaticity coordinates in the CIE 1931 chromaticity space of FIrpic, $Ir(mppy)_3$, PO-01-TB, and $Os(btfp)_2(pp2b)$ devices.

were later superimposed to simulate and predict the illumination properties of W-OLEDs.

2.2. Binary doping system

The dashed line in Fig. 2b shows the colour that are possible by combining the FIrpic ($(0.17, 0.35)_{CIE\ 1931}$) and $Os(btfp)_2(pp2b)$ ($(0.64, 0.36)_{CIE\ 1931}$) emission. Only one intersections between this line and the Planckian locus at $(0.33, 0.34)_{CIE\ 1931}$ was found to correspond to a CCT of 5700 K. Fig. 3a shows the simulated and experimental EL spectra of the R/B binary system W-OLEDs. The *J–V–L* curves and efficiency characteristics of the device are shown in Fig. 4, and the performances are summarised in Table 1. Although the device showed a promising performance with an EQE of 13.2%, power efficacy of 13.1 lm/W, and current efficiency of 22.6 cd/A with a $D_{u'v'}$ as low as +0.0034 at 1000 cd/m^2, the CRI value of this device was low (59) due to a concave feature at 560 nm in the EL spectrum.

2.3. Ternary doping system

To increase the CRI value, introducing a third emissive dopant into the EMLs that covers the green to yellow part of the lumination spectrum is reasonable [16,29–31]. The green-emitting dopant $Ir(mppy)_3$ and yellow-emitting dopant PO-01-TB are both suitable for this purpose. As shown in Fig. 5, white illumination with a CCT range from 5700 K to 2000 K can be obtained by introducing $Ir(mppy)_3$ (G) and PO-01-TB (Y) into the former R:B system. Interestingly, the R:G:B W-OLEDs showed the highest achievable CRI value of 83 at a low CCT near 2130 K ($(0.52, 0.41)_{CIE\ 1931}$), and the CRI value gradually decreased as the CCT increased, as shown in Fig. 5a. Conversely, the R:Y:B W-OLEDs showed a peak CRI value up to 81 at a CT of 3100 K ($(0.42, 0.40)_{CIE\ 1931}$), while the CRI values decreased both at CT > 3100 K and CT < 3100 K, as shown in Fig. 5b. The CRI values of the devices with a pre-determined CCT could be predicted with this simulation prior to the device fabrication and measurement. For instance, if an incandescent lamp-like W-OLED (CCT ~ 3000 K) is required, The R:G:B system yields a a CRI of 76, while R:Y:B W-OLEDs can potentially generate a CRI of 78. Accordingly, R:G:B and R:Y:B W-OLEDs with a CCT of approximately 3000 K were fabricated. As shown in Fig. 3b and c, the simulated and measured EL spectra showed little deviation, which indicated that the modelling can properly predict the illumination properties of the ternary devices. Fig. 4 shows the *J–V–L* curves and the efficiency characteristics of the ternary doping devices. Compared to the binary system, the R:Y:B ternary doping devices showed comparably high EQE values of 12.5%, a power efficacy of 14.3 lm/W and current efficiency of 22.5 cd/A at 1000 cd/m^2, while the R:G:B devices showed a slightly lower performance of 11.4% EQE, 10.6 lm/W and 20.8 cd/A at 1000 cd/m^2, which was presumably due to a lower quantum yield of $Ir(mppy)_3$ (70% measured in integrate sphere quantum yield measurement system).

2.4. Quaternary doping system

Modern lighting applications require high CRI values >80 [15,32]. In principle, these values can be reached by introducing a fourth or more emissive dopants into the EMLs of W-OLEDs. Compared to the co-evaporation technique in vacuum deposition, complicated doping ($\geqslant$4 dopants in a host) in a single EML is simplified with a solution process. To demonstrate this advantage, R:Y:G:B quaternary doping W-OLEDs were modelled and fabricated as shown in Fig. 6. In the quaternary doping system, the ratios of four components can be manipulated to ensure that the CIE coordinates of device emission are close to the Planckian locus. To simplify the modelling process, the ratio of red and blue components was first fixed as a starting point. As shown in Fig. 7, the starting points **A** to **F** represent the bluish to reddish spectra, which can be generated by FIrpic ($(0.17, 0.35)_{CIE\ 1931}$) and $Os(btfp)_2(pp2b)$ ((0.64,

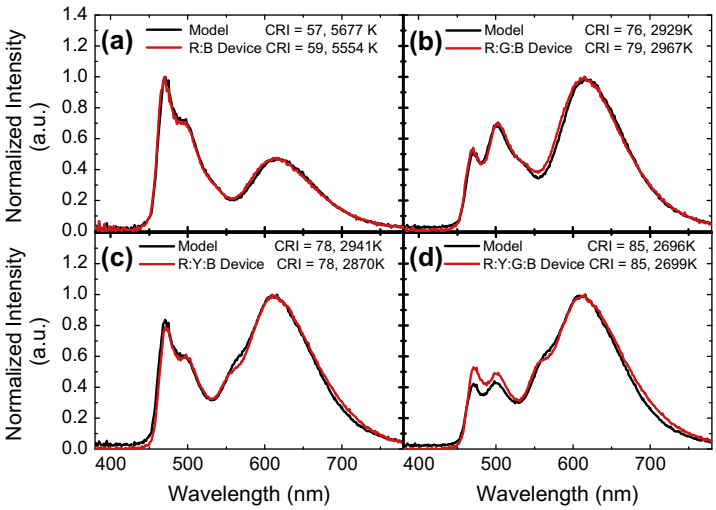

Fig. 3. Comparison between modelled and measured electroluminescence spectra of W-OLED devices: (a) R:B binary W-OELD, (b) R:G:B ternary W-OLED, (c) R:Y:B ternary W-OLED, and (d) R:Y:G:B quaternary W-OLED.

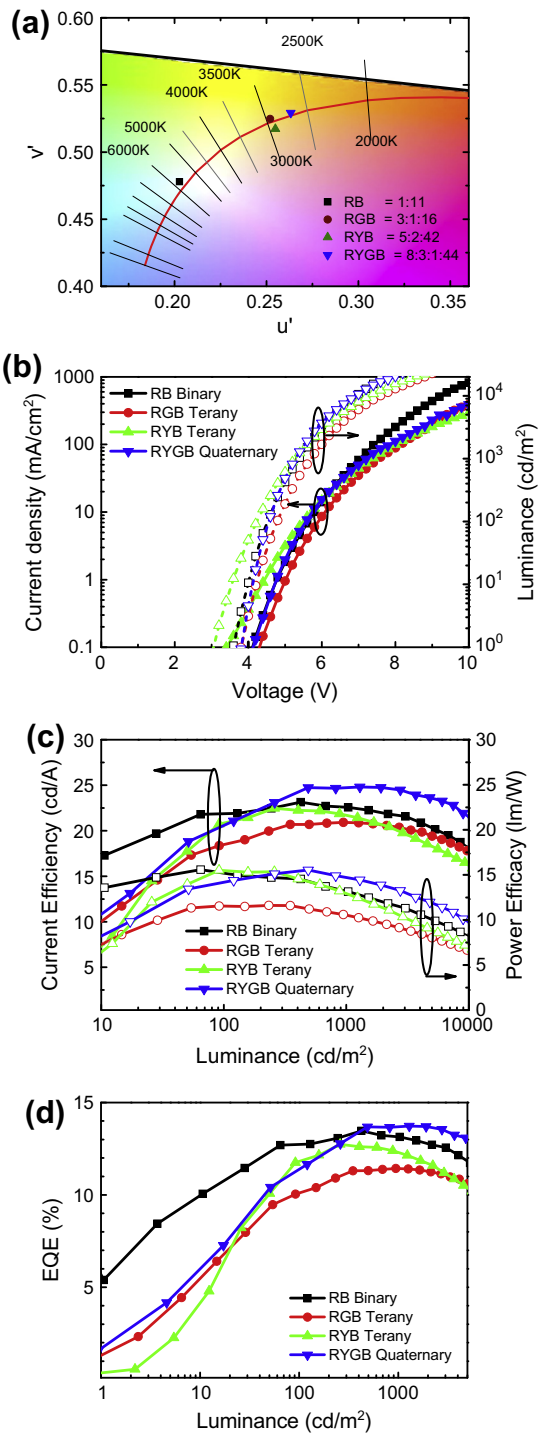

Fig. 4. (a) The chromaticity coordinates of the W-OLEDs in the CIE 1976 (L', u', v') colour space at different molecular weight ratios of dopants. (b) J–V–L characteristics, (c) current efficiencies and power efficacies, and (d) external quantum efficiencies of the W-OLEDs. (For interpretation of the references to colour in this figure legend, the reader is referred to the web version of this article.)

$0.36)_{\text{CIE 1931}}$) emission. The $D_{u'v'}$ values can be minimised and thus approaching the Planckian locus by adding a certain amount of Ir(mppy)$_3$ and PO-01-TB emission. The CIE coordinates (colour) and starting point-dependent CRI values are shown in the figures, and the highest achievable CRI values are indicated with red arrows. The simulation results show that the CRI values of quaternary doping W-OLEDs are generally higher than those of ternary W-OLEDs. A comparison of the highest CRI values in Fig. 7 shows that higher CRI value can be obtained at lower CCT values (87 (2291 K) > 85 (2696 K) > 84 (2854 K) > 83 (3114 K) > 81 (3499 K) = 81 (3464 K)). This indicates that the achievable highest CRI in quaternary W-OLED is still highly related to its CCT. The preferable high CRI results at lower CCT values could be due to the lack of deep blue emission for commercial available phosphorescence blue emitter (*i.e.* FIrPic). However, a CRI > 80 can be anticipated in R:Y:G:B W-OLEDs with a CCT range from 3500 K to 2000 K. Moreover, as in the binary and ternary systems, the highest achievable CCT value in the quaternary system is ~5700 K, limited by high CIE y value (0.35) of FIrpic. A wider CCT tunable range is anticipated if a blue dopant with emission of lower CIE y value ($\leqslant$0.28) is available. Figs. 3d and 4 show the EL spectrum and J–V–L characteristics of the CT = 2699 K quaternary device. As predicted by the simulation, the device not only showed the highest CRI value of 85 and a very small $D_{u'v'}$ value of +0.0009 but also possessed the best performance of 13.7% EQE, 14.7 lm/W and 13.6 cd/A at 1000 cd/m^2. A 30–40 lm/W of power efficacy is believed possible with the proper light extraction structures [9,33–36]. Device performance of the quaternary doping W-OLEDs with different CCT ranges from 4363 K to 2390 K is listed in Table 2. They all showed superior illumination properties than their binary and ternary counterparts of the same colour. The results indicate that multi-doping single EML W-OLEDs are promising candidates for efficient and high-quality lighting applications. Furthermore, as shown in S3, the colours of all WOLED devices were stable from 100 cd/m^2 to 3000 cd/m^2. A slight blue-shift occurred on each device operated above 10,000 cd/m^2. Fig. 8 shows a photo of the working quaternary doping and binary doping devices. Note the improved colour rendering capability of quaternary doping devices.

3. Conclusions

In summary, binary, ternary, and quaternary doping single EML W-OLEDs were comprehensively modelled. The relationship between CCT, CRI, and spectral designs was revealed. The simulation predicted that quaternary doping system show the best chromaticity performance. Solution-processed binary, ternary, and quaternary doping single EML W-OLEDs were fabricated and characterised to verify the numerical calculation. The experimental and simulated results closely approximate one another. Finally, a quaternary doping W-OLED with a CRI value up to 85, a $D_{u'v'}$ as low as +0.0009, an EQE of 13.7%, a power efficacy of 14.7 lm/W, and current efficiency as high as 24.6 cd/A at 1000 cd/m^2 was demonstrated. The methodology and implementation presented in this work should guide the future development of high CRI, low-cost, solution processed single EML W-OLEDs.

Table 1
Device performance of R:B, R:G:B, and R:Y:B W-OLEDs. The weight ratio of total dopants and host are fixed to 1:9.

Weight ratio of dopants in device fabrication	Ratio of EL spectrum in optical simulation	$\eta_{p,\ max}/\eta_{c,\ max}$/EQE (lm W^{-1}/cd A^{-1}/%)	$\eta_{p,\ 1000}/\eta_{c,\ 1000}$/EQE (lm W^{-1}/cd A^{-1}/%)	$CIE_{x,\ y}$	CCT (K)	CRI	$D_{u'v'}$
R:B	*R:B*						
1:11*	1:2.2	15.6/23.1/13.5	13.1/22.6/13.2	(0.33, 0.34)	5681	59	+0.0034
R:G:B	*R:G:B*						
3:1:8	12:3:1	10.6/17.0/10.9	8.8/16.9/10.8	(0.53, 0.41)	2011	83	-0.0015
3:1:16*	2:7:1	11.6/20.9/11.4	10.6/20.8/11.4	(0.44, 0.41)	2967	79	+0.0016
3:1:24	1:0.4:1.9	11.5/22.9/11.9	10.2/22.6/11.8	(0.33, 0.38)	5683	71	+0.0177
R:Y:B	*R:Y:B*						
1:1:6	1.8:2:1	17.3/25.9/12.5	15.9/25.0/12.2	(0.48, 0.43)	2627	75	+0.0058
3:1:16	3.1:1.1:1	14.0/18.7/10.4	12.9/18.6/10.4	(0.48, 0.40)	2428	80	-0.0046
4:1:20	2.2:0.8:1	16.4/26.6/12.9	14.2/26.2/12.7	(0.48, 0.39)	2366	78	-0.0079
5:2:42*	2:0.7:1	15.8/22.8/12.7	14.3/22.5/12.5	(0.45, 0.40)	2950	78	-0.0041

* The corresponding devices shown in Figure 4.

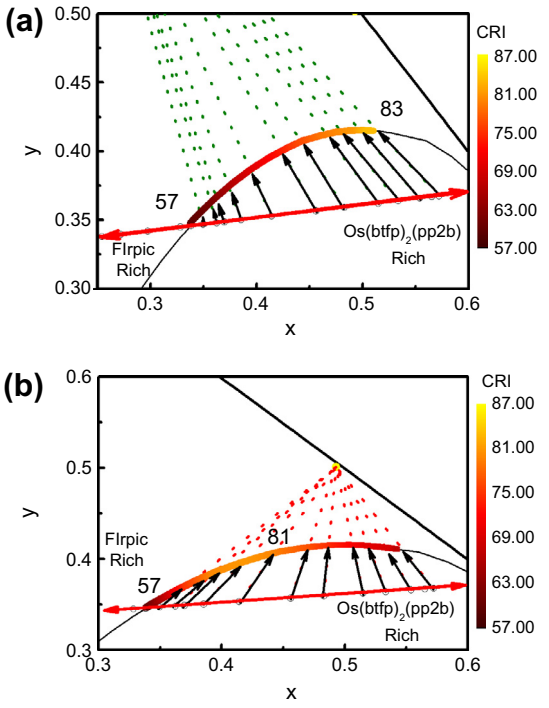

Fig. 5. Modelled CRI values of the ternary W-OLED. The Firpic and $Os(btfp)_2(pp2b)$ RB binary systems were used as the starting points and the desired chromaticity approaching the Planknian locus could be obtained by adding the third (a) $Ir(mppy)_3$ or (b) PO-01-TB dopants.

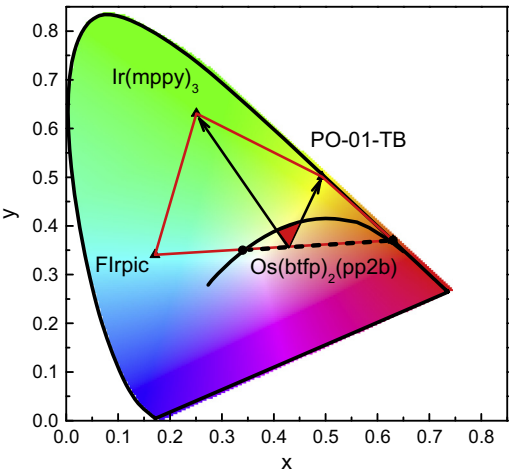

Fig. 6. Schematic of model simulating in quaternary case: the dashed line represents the section from $Os(btfp)_2(pp2b)$ (0.64, 0.36) to the intersection at (0.33, 0.34)*. The dashed line could be separated by several starting points from bluish (FIrpic-rich) to reddish ($Os(btfp)_2(pp2b)$-rich). Arrows pointing to $Ir(mppy)_3$ of (0.25, 0.63) and PO-01-TB of (0.49, 0.5) are constructed on one of these starting points. Because the arrows attach to the Planckian locus, a region of the CIE value that approaches the Planckian locus was obtained from the starting point as well as CRI value and correlated spectrum. *(The connection between FIrpic (0.17, 0.35) and $Os(btfp)_2(pp2b)$ (0.64, 0.36) intersects with Planckian locus at (0.33, 0.34)). (For interpretation of the references to colour in this figure legend, the reader is referred to the web version of this article.)

4. Experimental

4.1. Device fabrication

Indium tin oxide (ITO)-coated glass substrates were sequentially cleaned in an ultrasonic bath with de-ionised water, acetone, and methanol. The substrates were then treated with UV-ozone before thin film deposition. PEDOT:PSS was spin-coated onto the substrates, which were then dried in air at 135 °C for 30 min. A solution of TCTA (10 mg/mL) was prepared using toluene as a solvent and spin-coated onto the PEDOT:PSS layer. The cast films were baked at 100 °C for 10 min in a nitrogen atmosphere to remove the residual solvents. The emissive dopants and 26DCzPPy host were dissolved in toluene (6.67 mg/mL) and deposited by bar coating on a hot plate at 80 °C. The gap between the bar and the substrates was 60 μm, and the speed of the bar was controlled at 350 mm/s by an auto-bar coating machine. TmPyPB, CsF, and Al were thermally vaporised in a vacuum chamber with a base pressure $<10^{-6}$ Torr.

4.2. Measurements

The device characteristics were obtained by a Keithley 2636A source meter and silicon photodetector that was calibrated using a Photo Research, Inc. PR-650 SpectraScan

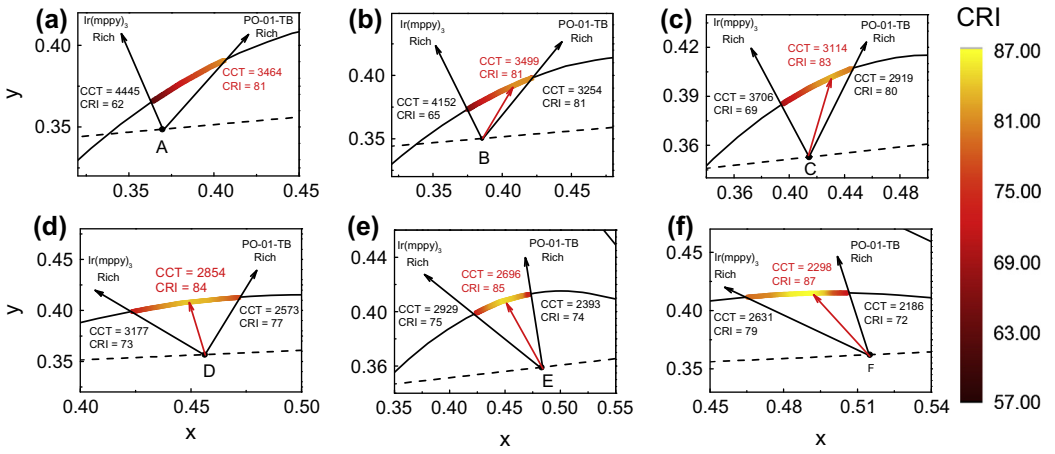

Fig. 7. Modelled CRI values of the quaternary W-OLED. The Firpic and Os(btfp)$_2$(pp2b) RB binary systems were used as the starting points (points A–F) and the desired chromaticity approaching Planknian locus could be obtained by adding Ir(mppy)$_3$ and PO-01-TB dopants.

Table 2
Device performance of R:Y:G:B W-OLEDs. The weight ratio of total dopants and host are fixed to 1:9).

Weight ratio of dopants in device fabrication	Ratio of EL spectrum in optical simulation	$\eta_{p,\ max}/\eta_{c,\ max}$/EQE (lm W^{-1}/cd A^{-1}/%)	$\eta_{p,\ 1000}/\eta_{c,\ 1000}$/EQE (lm W^{-1}/cd A^{-1}/%)	CIE$_{x,\ y}$	CCT (K)	CRI	$D_{u'v'}$
R:Y:G:B	*R:Y:G:B*						
5:1:1:42		15.4/21.7/10.5	13.5/21.0/10.2	(0.46, 0.44)	4363	79	+0.0179
10:3:3:84		15.8/21.7/10.5	14.6/22.2/10.3	(0.39, 0.43)	4095	80	+0.0199
5:2:2:50		17.2/23.3/12.1	16.1/24.9/11.9	(0.40, 0.43)	3970	82	+0.0191
10:4:3:84		14.4/19.5/8.6	13.5/19.3/8.5	(0.40, 0.44)	4034	82	+0.0232
5:2:4:42		17.9/24.6/10.2	15.5/24.1/10.2	(0.40, 0.46)	4002	74	+0.0294
6:2:1:42		13.7/19.5/10.7	11.8/19.0/10.4	(0.42, 0.42)	3368	83	+0.0076
8:3:1:44*	2:0.6:0.48:1	15.5/24.8/13.7	14.7/24.6/13.7	(0.47, 0.41)	2699	85	+0.0009
16:4:2:88		14.1/19.8/10.1	12.3/19.3/9.9	(0.48, 0.42)	2535	84	-0.0023
7:2:1:44		14.5/20.2/10.9	11.8/19.3/10.6	(0.48, 0.41)	2498	84	0.0000
8:3:1:48		14.5/21.3/11.4	12.2/20.9/11.2	(0.49, 0.42)	2390	83	-0.0001

* The corresponding devices shown in Figure 4.

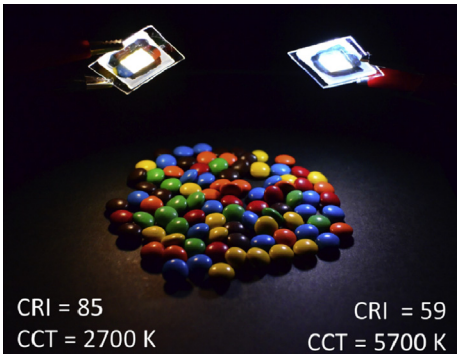

Fig. 8. Picture of the R:B binary and R:Y:G:B quaternary W-OLEDs. The R:B binary W-OLED exhibits cooler colour temperature at 5700 K and a low CRI value of 59 and the R:Y:G:B W-OLED showed a warm colour temperature at 2700 K with a high CRI value up to 85. (For interpretation of the references to colour in this figure legend, the reader is referred to the web version of this article.)

colorimeter. The electroluminescence (EL) spectra were measured by a calibrated Ocean Optics spectrometer. The thicknesses of each layer was measured with a V-VASE variable-angle spectroscopic ellipsometer (J. A. Woollam Inc.).

Acknowledgements

The work was financially supported by the National Science Council of Taiwan (NSC 101-2112-M-007-017-MY3, NSC 102-2221-E-007-125-MY3, NSC 102-2119-M-007-006) and the Low Carbon Energy Research Centre at the National Tsing-Hua University.

Appendix A. Supplementary material

Supplementary data associated with this article can be found, in the online version, at http://dx.doi.org/10.1016/j.orgel.2013.11.040.

Reference

[1] J. Kido, K. Hongawa, K. Okuyama, K. Nagai, Appl. Phys. Lett. 64 (1994) 815.
[2] H.-C. Yeh, H.-F. Meng, H.-W. Lin, T.-C. Chao, M.-R. Tseng, H.-W. Zan, Org. Electron. 13 (2012) 914.
[3] B. Zhang, G. Tan, C.S. Lam, B. Yao, C.L. Ho, L. Liu, Z. Xie, W.Y. Wong, J. Ding, L. Wang, Adv. Mater. 24 (2012) 1873.
[4] C. Huang, C.-G. Zhen, S.P. Su, Z.-K. Chen, X. Liu, D.-C. Zou, Y.-R. Shi, K.P. Loh, J. Organomet. Chem. 694 (2009) 1317.
[5] L. He, L. Duan, J. Qiao, D. Zhang, L. Wang, Y. Qiu, Org. Electron. 11 (2010) 1185.

[6] W. Mróz, C. Botta, U. Giovanella, E. Rossi, A. Colombo, C. Dragonetti, D. Roberto, R. Ugo, A. Valore, J.A.G. Williams, J. Mater. Chem. 21 (2011) 8653.
[7] T. Ye, S. Shao, J. Chen, L. Wang, D. Ma, ACS Appl. Mater. Inter. 3 (2011) 410.
[8] T. Fleetham, J. Ecton, Z. Wang, N. Bakken, J. Li, Adv. Mater. 25 (2013) 2573.
[9] S. Reineke, F. Lindner, G. Schwartz, N. Seidler, K. Walzer, B. Lussem, K. Leo, Nature 459 (2009) 234.
[10] H. Sasabe, J. Takamatsu, T. Motoyama, S. Watanabe, G. Wagenblast, N. Langer, O. Molt, E. Fuchs, C. Lennartz, J. Kido, Adv. Mater. 22 (2010) 5003.
[11] Y.-L. Chang, Y. Song, Z. Wang, M.G. Helander, J. Qiu, L. Chai, Z. Liu, G.D. Scholes, Z. Lu, Adv. Funct. Mater. 23 (2013) 705.
[12] J. Yu, H. Lin, F. Wang, Y. Lin, J. Zhang, H. Zhang, Z. Wang, B. Wei, J. Mater. Chem. 22 (2012) 22097.
[13] G. Schwartz, S. Reineke, T.C. Rosenow, K. Walzer, K. Leo, Adv. Funct. Mater. 19 (2009) 1319.
[14] S.O. Jeon, J.Y. Lee, Org. Electron. 12 (2011) 1893.
[15] S. Chen, G. Tan, W.-Y. Wong, H.-S. Kwok, Adv. Funct. Mater. 21 (2011) 3785.
[16] Y. Sun, S.R. Forrest, Appl. Phys. Lett. 91 (2007) 263503.
[17] G. Cheng, Y. Zhang, Y. Zhao, Y. Lin, C. Ruan, S. Liu, T. Fei, Y. Ma, Y. Cheng, Appl. Phys. Lett. 89 (2006) 043504.
[18] Y. Xu, J. Peng, J. Jiang, W. Xu, W. Yang, Y. Cao, Appl. Phys. Lett. 87 (2005) 193502.
[19] Q. Fu, J. Chen, C. Shi, D. Ma, ACS Appl. Mater. Inter. 4 (2012) 6579.
[20] Y.J. Doh, J.S. Park, W.S. Jeon, R. Pode, J.H. Kwon, Org. Electron. 13 (2012) 586.
[21] K.S. Yook, C.W. Joo, S.O. Jeon, J.Y. Lee, Org. Electron. 11 (2010) 184.
[22] H.-B. Wu, H.-F. Chen, C.-T. Liao, H.-C. Su, K.-T. Wong, Org. Electron. 13 (2012) 483.
[23] B.-S. Du, J.-L. Liao, M.-H. Huang, C.-H. Lin, H.-W. Lin, Y. Chi, H.-A. Pan, G.-L. Fan, K.-T. Wong, G.-H. Lee, P.-T. Chou, Adv. Funct. Mater. 22 (2012) 3491.
[24] S.-Y. Huang, H.-F. Meng, H.-L. Huang, T.-C. Chao, M.-R. Tseng, Y.-C. Chao, S.-F. Horng, Synth. Met. 160 (2010) 2393.
[25] X. Yang, D. Neher, D. Hertel, T.K. Däubler, Adv. Mater. 16 (2004) 161.
[26] R.J. Holmes, S.R. Forrest, Y.J. Tung, R.C. Kwong, J.J. Brown, S. Garon, M.E. Thompson, Appl. Phys. Lett. 82 (2003) 2422.
[27] Y. Ohno, Proc. of SPIE, 5530 (2004) 88.
[28] M.S. Rea, J.P. Freyssinier-Nova, Color Res. Appl. 33 (2008) 192.
[29] S. Nizamoglu, G. Zengin, H.V. Demir, Appl. Phys. Lett. 92 (2008) 031102.
[30] X. Qi, M. Slootsky, S. Forrest, Appl. Phys. Lett. 93 (2008) 193306.
[31] U.S. Bhansali, H. Jia, I.W.H. Oswald, M.A. Omary, B.E. Gnade, Appl. Phys. Lett. 100 (2012) 183305.
[32] M.C. Gather, A. Kohnen, K. Meerholz, Adv. Mater. 23 (2011) 233.
[33] W.H. Koo, W. Youn, P. Zhu, X.-H. Li, N. Tansu, F. So, Adv. Funct. Mater. 22 (2012) 3454.
[34] Q. Huang, K. Walzer, M. Pfeiffer, V. Lyssenko, G. He, K. Leo, Appl. Phys. Lett. 88 (2006) 113515.
[35] J.B. Kim, J.H. Lee, C.K. Moon, S.Y. Kim, J.J. Kim, Adv. Mater. 25 (2013) 3571.
[36] S.-Y. Kim, W.-I. Jeong, C. Mayr, Y.-S. Park, K.-H. Kim, J.-H. Lee, C.-K. Moon, W. Brütting, J.-J. Kim, Adv. Funct. Mater. 23 (2013) 3896.